Predicting Drying in Coatings that React and Gel: Drying Regime Maps

Richard A. Cairncross, Lorraine F. Francis, and L. E. Scriven
Dept. of Chemical Engineering and Materials Science, Center for Interfacial Engineering, and Minnesota Supercomputer Institute, University of Minnesota, Minneapolis, MN 55455

The competition between drying and reactions in a liquid coating containing precursors to a random network polymer can give rise to a variety of drying phenomena. Solidification, or gelation, of the polymer may occur before, after, or during the removal of solvents from the coating. Rates of drying and reaction are probed by solving the equations of mass transfer by diffusion along with chemical reaction in one dimension. Solutions to this system of equations are obtained by Galerkin's method with finite-element basis functions and entail large-scale computation. Skinning, or solidification at the surface of the coating while the bulk is still liquid, occurs in thick coatings when the diffusional resistance to drying is significant, that is, at high mass-transfer coefficients. Homogeneous solidification occurs in thin coatings at low mass-transfer coefficients. Drying regime maps represent these solidification phenomena as regions in parameter space.

Introduction

Controlled solidification of a liquid solution or suspension coating is essential in making many products. In photographic coatings, gelatin solutions solidify at first by cooling; in water-borne paints, colloidal latex suspensions solidify by drying and film-forming coalescence; in solvent coatings, solutions solidify by drying, cooling, or cross-linking reactions; in plastisol coatings, polymeric suspensions begin solidifying by heating; in asymmetric membranes, polymer solutions phase separate into bicontinuous structures by extraction that is often preceded by limited drying; in ceramic coatings by the sol-to-gel route, precursor solutions transform into molecular or colloidal gel by hydrolysis and polymerization accompanied by solvent evaporation (Cohen, 1990; Anderson and Ullman, 1973; Vrentas et al., 1985). In every case, the solidification process affects the development of the desired final coating properties and microstructure (Anderson and Ullman, 1973; Tsay and McHugh, 1990; Brinker et al., 1990). When drying and reaction are not adequately controlled, the solidified coating fails or is defective. Examples of failure are delamination and massive cracking. Examples of defects are crazing, curl and cockle, bubbles and craters, local variation in composition or microstructure, and unacceptable levels of residual solvent or monomer (Pierce and Schoff, 1988; Calbo, 1987; Hahn, 1987).

Often the rate of solidification governs the level of defects or the onset of failure. Then the speed of coating and solidifying in a manufacturing facility is limited by drying and reaction. A useful tool for coping with the limitation is a theory of solidification by drying and reaction that accurately predicts observation in representative experiments, and so can be used to choose process conditions that yield a defect-free coating of desired composition, microstructure, and properties. Such a tool for design and troubleshooting is the goal of this article.

Specifically, this article treats the combined effects of drying and reaction in random network polymerizing solutions, with a special focus on a polymerizable metal alkoxide solution. The metal alkoxide solution is tetramethoxysilane–methanol–water–hydrochloric acid, here called a *TMOS sol*. It reacts to form loosely branched polymers and eventually *gels* into a porous network filled with solvent; ultimately, the gel can be dried and heat-treated to form a silicon dioxide ceramic. This is an example of *sol-gel* processing to form ceramic materials (Brinker and Scherer, 1990). The liquid coating can be regarded as having gelled, and thereby solidified, when the average polymer size seems to diverge to infinity, that is, a sample-spanning polymer forms. The theory

Correspondence concerning this article should be addressed to L. E. Scriven. Present address of R. A. Cairncross: Mechanical Engineering Dept., University of Delaware, Newark, DE 19716.

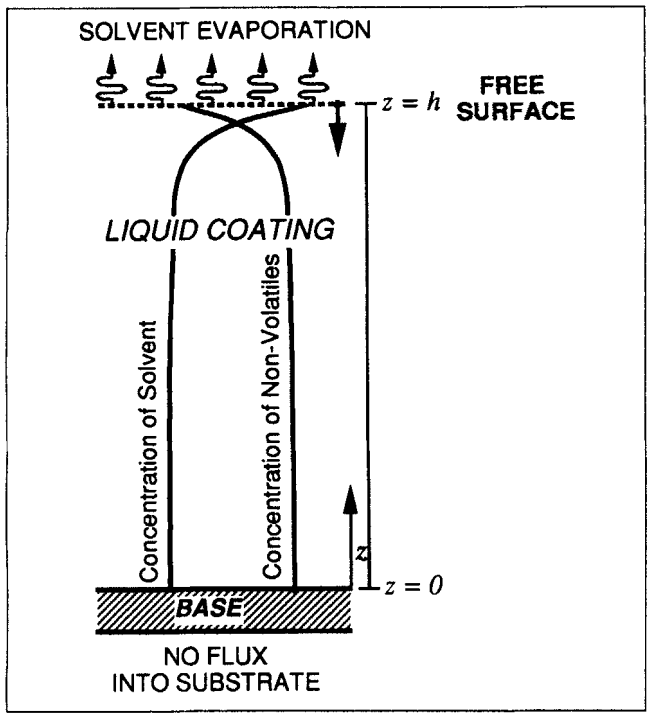

Figure 1. Coated film and the 1-D domain used in the theory of drying and reacting coatings.

worked out here applies strictly only to the solidification process up to a stage a little short of gelation. Nevertheless, the theory is applied, less rigorously, to a period of postgelation drying and reaction. This is done simply by extending the same constitutive equation for diffusion into the period after gelation. This theory predicts the extent to which a coating dries prior to gelation.

When evaporation and reaction proceed on about the same time scale, they can interact to produce a phenomenon called *skinning*. When evaporation is not limited by the external conditions of gas flow and vapor concentration, the concentrations of evaporating reactants and products vary with depth. The water of the TMOS system is both a reactant (in hydrolysis steps) and a product (in condensation steps); moreover, the second volatile solvent, methanol, is also a product. Both are more volatile than TMOS itself. Usually the reactants become more concentrated near the drying surface than in the bulk of the coating. Consequently, the reactions accelerate near the drying surface, and the mean molecular weight of polymeric products near the drying surface rises faster than deeper within the coating (Cairncross et al., 1992). Eventually this leads to gelation of solution near the drying surface before gelation of solution deeper within the coating, a phenomenon here called *literal skinning* (Cairncross, 1994). Skinning is often seen, especially in asymmetric phase inversion membrane production, but is not necessarily caused by gelation reactions (Anderson and Ullman, 1973). And literal skinning need not imply that evaporation is halted or that a drier coating would result if skinning were avoided (Powers and Collier, 1990); it merely means that a fraction of the coating is solid while a fraction is still liquid for an appreciable time. Literal skinning can occur as a result of any solidification process that is enhanced by removal of volatiles from the solution. The theory put forth in this article predicts when skinning may occur.

This article is divided into three sections. The first outlines the equations of diffusion, evaporation, and reaction within a coating. Two kinetic schemes are reviewed that describe the reactions leading to gelation of acid-catalyzed TMOS solutions. Methods are given for predicting polymer molecular weights in both of the kinetic schemes. The second section reports representative predictions of drying in TMOS coatings and analyzes the mechanisms that control the evaporation and gelation. The third section presents maps of gelation, skinning, and drying vs. the key reaction rate constant (in a Damköhler number) and the convective mass-transfer coefficient (in a Biot number) of the gas stream sweeping the TMOS coating. How these maps vary with the definitions of gelation and skinning is discussed, as is their sensitivity to the vapor–liquid equilibrium coefficients and diffusion coefficients.

Theory

• Equations for evaporation and reaction

Drying of a coated liquid film without transverse variation in composition or coating thickness can be described by the one-dimensional convection-diffusion-reaction equation (Cairncross et al., 1992; Cairncross, 1994; and Vrentas et al., 1985) with appropriate boundary conditions (Figure 1):

$$\frac{dx_i}{dt} + v^n \frac{\partial x_i}{\partial x} - \frac{\partial}{\partial z}\left(D_i \frac{\partial x_i}{\partial z} \right) = R_i \tag{1}$$

$$D_i \frac{\partial x_i}{\partial z} = 0 \text{ at substrate } (z = 0) \tag{2}$$

$$- D_i \frac{\partial x_i}{\partial z} - x_i v^s = \hat{V}_i K_{Gi} (\rho_i^{gs} - \rho_i^{g\infty}) \text{ at free surface } (z = h) \tag{3}$$

$$v^s = - \sum_{i=1}^{n} \hat{V}_i K_{Gi} (\rho_i^{gs} - \rho_i^{g\infty}) \text{ at free surface } (z = h). \tag{4}$$

This equation set corresponds to an isothermal coating with no flux into the substrate. The time rate of change of volume fraction, x_i, of species i by convection, diffusion, and reaction in a field of reference points moving at velocity v^n is dx_i/dt. The distance from the reference plane at the substrate–coating interface is z. The diffusive flux is described by Fick's law relative to the volume-averaged velocity in multicomponent solutions with the cross-term diffusion coefficients set to zero; D_i is the diffusion coefficient of species i; R_i is the volumetric production of species i by reactions. This equation set incorporates ideal solution behavior and volume-conserving reactions; so there is no volume change on mixing or reaction. These restrictions combined with Eq. 2 result in no volumetric motion of the liquid; thus, the volume-averaged velocity is zero. The movement of reference points used in numerical solution of these equations is represented by v^n. The specific volume of pure component i is $\hat{V}_i$. Mass flux through the gas above the coating is described by a mass-transfer coefficient, K_{Gi}, and a driving force, $(\rho_i^{gs} - \rho_i^{g\infty})$. The concentration of solvent in the gas at the free sur-

Table 1. Typical Parameter Values of Acid-Catalyzed Tetramethoxysilane Sols

$h_0 = 0.001$ cm	Ref. coating thickness	$\rho_{liq} = 1$ g/cm^3	Ref. liquid conc.
$D_0 = 10^{-6}$ cm^2/s	Ref. diffusivity	$\rho_{gas} = 0.000215$ g/cm^3	Ref. gas conc.
$t_0 = h_0^2/D_0 = 1$ s	Ref. time unit	$\hat{V}_1 = 1.0$ cm^3/g	Sp. vol. of pure water
$K_G = 5$ cm/s	Mass-transfer coeff.	$\hat{V}_2 = 1.26$ cm^3/g	Sp. vol of pure methanol
$k_{r0} = 1$ cm^3/g/s	Ref. reaction rate const.	$\hat{V}_3 = 0.97$ cm^3/g	Sp. vol. of pure TMOS
Reaction Rate Constants		First Shell Substitution	Independent Reactions
Hydrolysis rate constant	k_h	3.33 cm^3/mol/s	3.33 cm^3/mol/s
Water condensation rate constant	k_w	0.1 cm^3/mol/s	0.0086 cm^3/mol/s
Alcohol condensation rate constant	k_a	0.016 cm^3/mol/s	0.00152 cm^3/mol/s
Substitution effect factor	R	0.35	not applicable
$Da = \frac{h_0^2 \rho_{liq} k_{r0}}{D_0} = 1$	Damköhler number reaction rate/diffusion	$Bi = \frac{K_G h_0 \rho_{gas}}{D_0 \rho_{liq}} = 1$	Biot no.: internal/external mass-transfer resistance

face, ρ_i^{gs}, is related to the solvent concentration in the liquid at the free surface by Raoult's law, and $\rho_i^{g\infty}$ is the concentration of solvent far away in the gas (normally this is set to zero). The mass flux in the gas provides a boundary condition on the convection-diffusion-reaction equation, Eq. 1 and an equation, Eq. 4, for the free surface velocity v^s, which is the rate of change of thickness of the coating, dh/dt.

Standard values of parameters of the acid-catalyzed tetramethoxysilane (TMOS) sol are shown in Table 1. For numerical solution, Eqs. 1 to 4 are scaled as shown in an earlier report (Cairncross et al., 1992). The results are most sensitive to the Biot number and the Damköhler number which are defined in Table 1. The *Biot number* is the ratio of the internal mass-transfer resistance to the external mass-transfer resistance. The *Damköhler number* is the ratio of a reference reaction rate to the diffusion rate. Because many reactions may occur in one solution, the Damköhler number represents a standard scaling for all of them. In this article, the Damköhler number and Biot number are varied over many orders of magnitude, which corresponds to varying any of the parameters in their definition. For specific chemical systems, it is convenient to view the Damköhler number as relating to coating thickness (actually coating thickness squared) and the Biot number as relating to the mass-transfer coefficient, or to the airflow responsible.

The drying characteristics predicted by this theory are sensitive to the diffusivities, chemical kinetics, mass-transfer coefficients, and vapor–liquid equilibrium of solvents. The mass-transfer coefficients can be predicted by standard correlations and so are not discussed further here. The partial pressures of solvents in the gas are in equilibrium with the liquid solvent at the surface of the coating and are described by Raoult's law.

In solutions that solidify or gel, the diffusion coefficients are lower in the gel than in the sol, but the magnitude of the differences depend on the microstructure of the gelled material and the mobility of solvent and polymers within the solid matrix. In polymers undergoing a glass transition, the diffusion coefficient drops many orders of magnitude; likewise in materials that crystallize, the diffusion coefficient drops nearly to zero. However, during gelation, the magnitude of the change in diffusion coefficient is less certain; some gelled membranes offer virtually no additional resistance to solvent diffusion whereas others nearly shut off diffusion (Cussler, 1984). Also, experimental evidence indicates that the diffusion coefficients are often time-dependent; that is, they depend on relaxation of polymeric species (Frisch, 1989; Crank and Park, 1951; Long and Richman 1960). Thus, prediction of diffusion coefficient variation with concentration and molecular weight (even in isothermal solutions) in gelling solutions is complicated (Vrentas and Duda, 1977). In addition, experimental determination of diffusivities is difficult, and literature on solvent diffusivities in gelling solutions is scarce. Throughout most of this article, the predictions use a constant diffusion coefficient which is the same for all the species in solution.

Method of computer-aided solution of the equations

The system of equations (Eqs. 1 to 4) is solved in a straightforward way by Galerkin's method and quadratic, one-dimensional finite-element basis functions (Strang and Fix, 1973; Finlayson, 1992). This method yields a system of nonlinear ordinary differential equations for the coefficients of the quadratic basis functions. The coating is divided into 10 finite elements with quadratic interpolation of the concentrations of each chemical species across each element; there are 21 basis functions and one unknown for each chemical species associated with each basis function. Three-point Gaussian quadrature is used to evaluate the weighted residuals. The system of nonlinear ordinary differential equations is solved by DASRT (Petzold, 1982; Brenan et al., 1989), a powerful nonlinear differential and algebraic equations system solver with automated time stepping and a variable-order, backward-difference approximation. On a Cray Y-MP supercomputer, the results in this article used 5 s to 1 min of computer time to integrate from initial wet coating to final dry coating, depending on the number of chemical species involved.

Kinetics in gelling solutions

In many sol-to-gel systems, alkoxide monomers hydrolyze and condense into a network polymer. Acid-catalyzed tetramethoxysilane [TMOS, or $Si(OCH_3)_4$] reacts to form a polymeric silicate gel. In hydrolysis, a methoxyl functional group on silicon is replaced by a hydroxyl one through reaction with water and formation of byproduct methanol: $R_3Si\text{-}OCH_3 + H_2O \Leftrightarrow R_3Si\text{-}OH + CH_3OH$; here R represents any attached functional group. In condensation, oxygen bridges are formed

between silicon atoms with production of byproduct water or methanol: $R_3Si\text{-}OH + R_3Si-OH \Rightarrow R_3Si\text{-}O\text{-}SiR_3 + H_2O$ and $R_3Si\text{-}OCH_3 + R_3Si\text{-}OH \Rightarrow R_3Si\text{-}O\text{-}SiR_3 + CH_3OH$. The important features of this kinetic scheme are as follows: solvents are produced by the reactions with a production of four methanol molecules for every TMOS monomer and net consumption of two water molecules for every TMOS monomer, and condensation reactions build up branched polymers.

The essential features of these hydrolysis and condensation reactions are captured in a simple kinetic scheme based on independent reactivity of functional groups; that is, an alkoxide or hydroxide on a monomer reacts at the same rate as an alkoxide or hydroxide on a large polymer. Thus, the species in the chemical kinetics are the functional groups attached to silicon. We refer to this simple scheme as *independent reactions*:

$$Si\text{-}OCH_3 + H_2O \underset{k_h}{\overset{k_h}{\rightleftarrows}} Si\text{-}OH + CH_3OH \qquad \text{(Hydrolysis)}$$

$$Si\text{-}OH + Si\text{-}OH \overset{k_w/2}{\Rightarrow} 2\,Si[O\text{-}Si] + H_2O$$

(Water-producing condensation)

$$Si\text{-}OCH_3 + Si\text{-}OH \overset{k_a/2}{\Rightarrow} 2\,Si[O\text{-}Si] + CH_3OH$$

(Methanol-producing condensation)

This kinetic scheme uses only five chemical species: water, methanol, unreacted alkoxide units ($Si\text{-}OCH_3$), hydrolyzed units (Si-OH), and condensed units (Si[O-Si]); in each of these chemical species, the other three functional units attached to the silicon atom are ignored. Only four reactions can occur in this kinetic scheme (including reversible hydrolysis); hence, only four rate constants are required (Kay and Assink, 1988). Thus, one TMOS molecule is represented by four unreacted units, and one SiO_2 structural unit is represented by four condensed units. The independent reaction scheme qualitatively predicts the concentrations of condensed species in the acid-catalyzed TMOS solution, which can be measured by NMR (nuclear magnetic resonance spectroscopy).

In another scheme, Kay and Assink (1988) assume that the susceptibility of the oligomeric units around each silicon atom to these reactions depends solely on the four nearest neighbor functional groups (Figure 2); this dependence is often called a *first shell substitution effect*. The Kay and Assink scheme incorporates fifteen different Si-species in the chemical kinetics that react by 165 second-order hydrolysis and condensation reactions. *Kay and Assink's statistical reaction scheme (first shell substitution)* generates the needed 165 rate constants from four independent parameters (Kay and Assink, 1988; Assink and Kay, 1988; Brinker and Assink, 1989; and Bailey et al., 1990), including a substitution factor R, which is the ratio of rate constants of each successive condensation reaction. When R = 1, there is no substitution effect; so independent reactions and first shell substitution predict equal overall rates of hydrolysis and condensation and predict equivalent gelation times (see below). Improved kinetic schemes and constants have been developed by Sanchez et al. (1992, 1994, 1996) and Abhiraman (1994) for tetraethoxysilane (TEOS); they used nuclear magnetic resonance (NMR) measurements and modeling to determine the individual reaction rate constants of the reactions they observed, including temperature dependence and reversible hydrolysis.

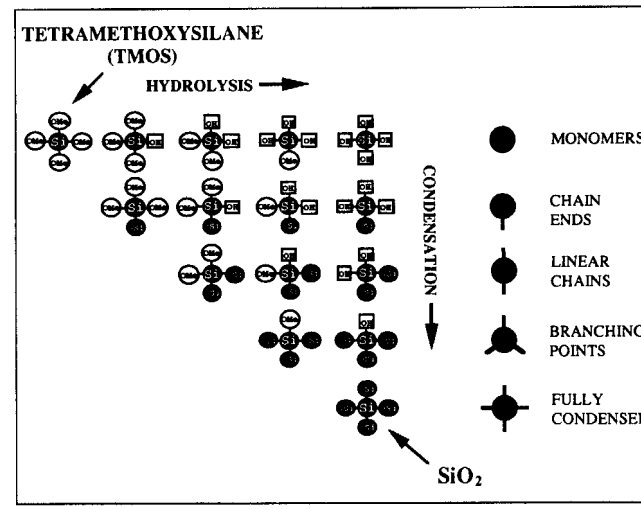

Figure 2. Functional group representation of kinetics of reaction of TMOS to produce silica polymers in acid-catalyzed tetramethoxysilane (TMOS) solutions (from Kay and Assink, 1988).

This scheme has 15 Si-species and 165 reactions. Each row of silica species represents a certain contribution to polymer structure.

Prediction of gelation

From both of the preceding kinetic schemes, the average molecular weight of the branched polymers in solution can be estimated by statistical methods based on those of Flory (1953), Macosko and Miller (1976), and Bailey et al. (1990). Their approximations neglect intramolecular reactions (cross-links) and assume independent reactivity of similar chemical species. The assumption of no cross-links is plainly incorrect for gelled polymers, but normally introduces only small errors prior to gelation. For independent reactions the molecular weight of the polymer is calculated from the conversion, p, the fraction of functional groups that have condensed:

$$p \equiv \frac{\text{mol of condensed functional groups}}{\text{total mol of functional groups}} = \frac{[Si{-}OSi]}{4\,[Si]}. \quad (5)$$

The monomers each have four functional groups. [Si–OSi] is the molar concentration of functional groups that have condensed to form siloxane bonds; this number is equal to twice the molar concentration of siloxane bonds because each siloxane bond connects two functional units. [Si] is the total concentration of silicon atoms in solution. Likewise, the fraction of functional units that are hydroxide and alkoxide units can be calculated and labeled p_{OH} and p_{OR}, respectively. The weight-averaged molecular weight $\bar{M}_w$, of polymers resulting from solvent-producing condensation reactions is calculated from the recursive method of Macosko and Miller (1976):

$$\bar{M}_w \equiv \frac{1}{1-3p}[(1+p)M_m + 4\,p_{OH}M_{OH} + 4\,p_{OR}M_{OR}]. \quad (6)$$

The molecular weights of SiO_2, hydroxide functional units, and alkoxide functional units are $M_m = 60$, $M_{OH} = 9$, and $M_{OR} = 23$ g per mole, respectively (Bailey et al., 1990). In Eq. 6, the molecular weight diverges to infinity when the denominator of the coefficient goes to zero, $p_{gel} = 1/3$; so this theory predicts that silica polymers gel at 33% conversion.

For first-shell substitution, Bailey et al. (1990) generalized the recursive method of Macosko and Miller (1976) to calculate the weight-averaged molecular weight from the known concentrations and molecular weights of the fifteen different Si-species. In their theory, the polymer gels when the number of expected siloxane bonds on silicon atoms that are not monomers (condensed at least once), D_3, is equal to unity:

$$D_3 \equiv \sum_{i=1}^{4}\sum_{j=0}^{4-i} P(Q_i^j)(i-1), \quad (7)$$

Here, $P(Q_i^j)$ is the weight-averaged probability of selecting a Si-species of type Q_i^j from the ensemble of Si-species that are condensed at least once, where i is the number of siloxane bonds, j is the number of hydroxide bonds on the atom, and $i \geq 1$:

$$P(Q_i^j) \equiv \frac{ix(Q_i^j)}{\sum_{i=1}^{4}\sum_{j=0}^{4-i} ix(Q_i^j)}. \quad (8)$$

The mole fraction of each species is $x(Q_i^j)$. Bailey et al. (1990) have shown that the extent of conversion when the molecular weight diverges depends on the substitution effect factor, R, in first-shell substitution. Kinetics with a first-shell substitution effect ($R < 1$) predict a larger concentration of species with lower coordination (or connectivity); this results in gelation at a higher conversion. For $R = 0.35$, which is suggested by Bailey et al. (1990) and Brinker and Assink (1989), gelation occurs at 44% conversion (Figure 3).

Comparison of kinetic schemes without drying

Figure 3 shows the predicted conversion (fraction of functional units that have condensed) vs. time without drying. The first-shell substitution effect ($R = 0.35$) causes the reaction rate to drop well below the reaction rate with no substitution effect ($R = 1$). The condensation rate constants in the independent reaction scheme were determined to match the predicted gelation times without drying with a first-shell substitution effect ($R = 0.35$). We used a Picard iteration to determine the rate constants listed in Table 1 (for $R = 0.35$); so the predicted gelation times without drying were within 1% of each other for the two schemes. Because the independent reaction scheme does not include a substitution effect, the effective condensation rate constant is lower, and the conversion, or the fraction of reactive sites that have condensed, initially rises more rapidly for first shell substitution than for independent reactions. However, the conversion in first-shell substitution plateaus whereas the conversion in independent

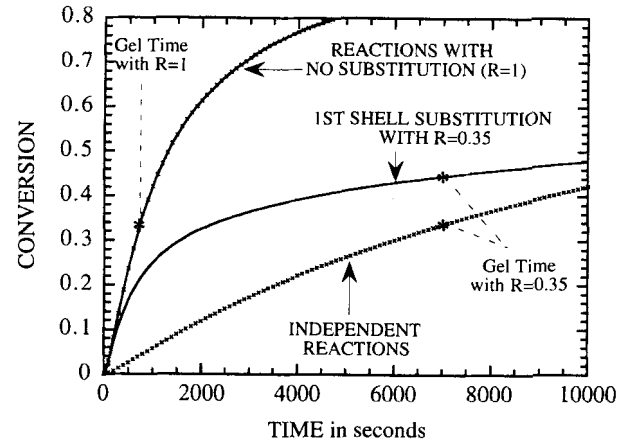

Figure 3. Conversion by reactions without drying as predicted by first shell substitution (lines) and by independent reactions (x's).

Results are shown for no substitution effect ($R = 1$), $R = 0.35$, and an independent reaction approximation to first shell substitution with $R = 0.35$ based on equal gelation time.

reactions continues to rise as shown in Figure 3. Thus, more solvent is produced early with the first shell substitution reactions, but later the independent reactions achieve a higher extent of conversion. Also, gelation occurs at a conversion of one-third for independent reactions, whereas it does not occur until a conversion of about 0.44 for first-shell substitution, because condensation at the ends of polymer segments is favored over formation of branches.

The gelation point predicted by Eqs. 6 and 7 occurs when the polymer molecular weight diverges to infinity. In solutions without drying, the time-to-gelation depends upon the starting composition, as shown in Figure 4. The first-shell substitution delays gelation because condensation reactions

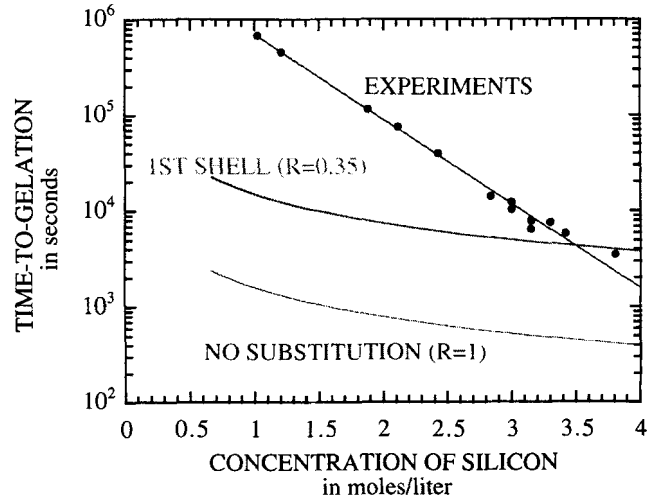

Figure 4. Predicted time-to-gelation based on first-shell substitution vs. no-substitution kinetics at varying initial concentration of tetramethoxysilane in absence of drying.

Experimentally measured time-to-gelation is much more sensitive to concentration than the theory predicts (Limbert, 1993).

are slower. Because these kinetic schemes are second-order, they show a squared dependence on the starting composition. The time-to-gelation, measured as the time at which the solution no longer flows during our sampling time (~ 1 min) depends exponentially on the TMOS concentration (Limbert, 1993). Thus, the experimentally observed time-to-gelation depends much more strongly on solution composition than the theoretically predicted time-to-gelation based on independent reactions and first-shell substitution.

There are several possible explanations for this discrepancy between theory and experiment, which come from the chemical kinetics, the prediction of gelation, and the relationship between predicted gelation and observed gelation. Both kinetic schemes, namely independent reactions and first shell substitution are second-order, which means the reaction rates depend upon the square of the reactant concentration. These schemes are accurate in describing the kinetics of the reactions in the initial stages, but become increasingly less accurate near the gelation point (Bailey et al., 1990). Indeed, the kinetics of the reactions in the later stages of gelation may not be second-order. Several researchers (Ng et al., 1995; Sanchez et al., 1996; Abhiraman, 1994) are improving these kinetics to include reversible hydrolysis reactions, better rate constants, and cycle formation by acid catalyzed tetramethoxysilane and tetraethoxysilane sol-to-gel reactions.

Independent reactions and first shell substitution predict gelation at 0.33 and 0.44 conversion, respectively; however, experimental results of Sanchez and McCormick (1994) show gelation at about 0.8 conversion in TEOS sols. The network polymer theories used to derive Eqs. 6 and 7 result from assuming independent reactivity of similar functional units and absence of intramolecular reactions, that is, no crosslinking, cycle, and multicycle formation. Several researchers have shown that cycles form in TMOS and TEOS solutions; so the assumptions of these polymer network theories are not strictly valid for these solutions. Also, the macroscopic gel point, measured by observing when the solution no longer flows on an appreciable time scale, does not necessarily correspond to the time at which the polymer molecular weight diverges to infinity. Entanglements between large polymers may cause observed gelation before infinite molecular weight is reached, while breakage of bonds may cause observed gelation after infinite molecular weight is reached.

Nevertheless, these kinetic theories do qualitatively reproduce the trends seen in the experimental data. Likewise, the experimentally measured time-to-gelation without drying (Figure 4) can be used to model empirically the gelation kinetics. Because the time-to-gelation depends exponentially on the starting composition, the characteristic rate of condensation reactions depends exponentially on the starting composition. Thus, *empirical models* of gelation reactions can be defined; in this article we consider two such models. The first empirical model assumes that gelation occurs when the time-to-gelation, which corresponds to the concentration of silicon species in solution (Figure 4), is less than the time since the solution was mixed:

$$t_{\text{gel}}(C_{\text{Si}}) = 89{,}347 \exp(-2.0376\, C_{\text{Si}}), \tag{9}$$

Here, C_{Si} is the total concentration of silicon in the solution in moles per liter, and $t_{gel}(C_{\text{Si}})$ is the time-to-gelation in minutes. Equation 9 is a curve fit to the experimental data in Figure 4. The second empirical model assumes that the rate of condensation reactions is proportional to the inverse of the experimentally measured time-to-gelation at the concentration of silicon species in the solution. For a first-order kinetic scheme, with the assumption that hydrolysis reactions are complete, this empirical model is

$$R_{\text{OH}}^{\text{cond}} \equiv -k_c(C_{\text{Si}})[C_{\text{OH}}] \tag{10}$$

$$k_c(C_{\text{Si}}) \equiv \frac{-\ln(1-p_{\text{gel}})}{t_{\text{gel}}(C_{\text{Si}})}, \tag{11}$$

where $R_{\text{OH}}^{\text{cond}}$ is the rate of condensation reactions, C_{OH} is the concentration of hydroxide functional units, k_c is the condensation rate constant that is a function of C_{Si}, p_{gel} is the conversion at gelation, and t_{gel} is the time to gelation from Eq. 9. The straight line in Figure 4 defines the function $t_{\text{gel}}(C_{\text{Si}})$. This kinetic scheme can be substituted in the drying equations, (Eqs. 1–4). These empirical models are discussed in more detail later.

Prediction of Drying and Reaction

Case study — Comparing kinetic schemes

In this section the predictions of the independent reaction kinetic scheme and the first-shell substitution kinetic scheme are compared. The simplified scheme (independent reactions) qualitatively reproduces the characteristics of the first shell substitution scheme and clarifies the mechanisms involved. In all of the results shown below, the initial solution contains 2.2 moles per liter of TMOS, 8.8 moles per liter of water (hydrolysis ratio, $R_w = 4$), and the balance of the solution is methanol. The physical parameters listed in Table 1 are typical values of acid-catalyzed TMOS solutions. The reaction rate constants of first-shell substitution were determined experimentally by Kay and Assink (1988). The independent reaction rate constants are listed in Table 1, and predict gelation time equal to the first-shell substitution without drying.

Figure 5 shows a comparison between the two schemes for a drying coating with $Da = 100$; Da is the Damköhler number, which represents the ratio of rate of reaction to rate of diffusion. Initially, both schemes predict about the same drying rate. However, first-shell substitution predicts faster solvent production due to faster initial condensation reactions, and the first-shell substitution coating eventually dries faster than the independent reactions coating. Faster drying accelerates reactions more, and first-shell substitution predicts a shorter gelation time than independent reactions. The dashed lines in Figure 5 represent the place in the coating where the predicted molecular weight of the silica polymers diverges to infinity. Numerically this occurs when the conversion equals one-third for independent reactions (Eq. 6) and when D_3 equals unity for first-shell substitution (Eq. 7). During the period in which this place migrates through the coating, material above the dashed line is solid while material below it is still liquid, a case of literal skinning. In all of the results in this article that indicate literal skinning, the gelation occurs

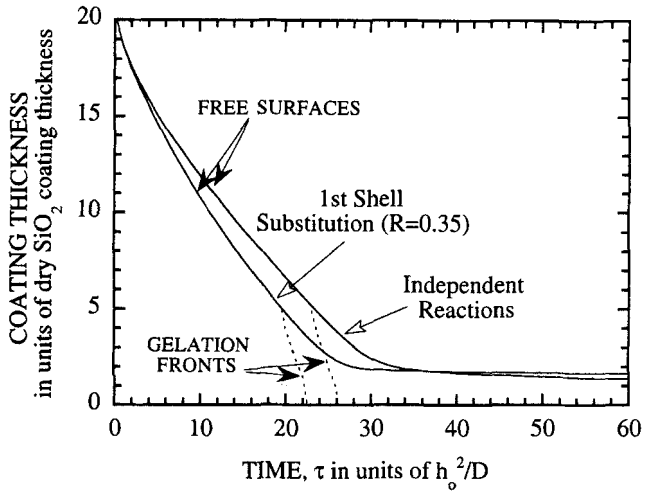

Figure 5. Drying vs. gelation in a coating reacting with first-shell substitution ($R = 0.35$) vs. independent reactions.

Both results correspond to Damköhler number, $Da = 100$, and Biot number, $Bi = 1$.

first at the free surface of the coating, and then propagates across the coating in a front represented by the dashed line. The final coating thicknesses predicted by both schemes are approximately the same.

Figures 6a and 6b show volume fraction profiles of nonvolatile Si-species (the sum of volume fractions of all the Si-species) across the coating at a sequence of times. The solvent produced by reactions causes the volume fraction of nonvolatile Si-species to fall initially. The sharp rise in the concentration near the free surface is called *diffusional*, or *figurative, skinning*, indicating that mass transport of solvents to the free surface is limited by diffusion; the nonvolatile Si-species accumulate there as the solvents depart. The magnitude of the diffusional skinning (the concentration difference between the free surface and base) rises sharply early in drying, then levels, and later decreases as solvents are depleted. Figures 5 and 6 show that first-shell substitution and independent reactions predict qualitatively similar changes in coating thickness, gelation, and gradients of Si-species. For the purpose of this article, qualitative agreement of gelation and drying times between the schemes is sufficient to illustrate the mechanisms involved and to generate drying regime maps.

The predicted coating thickness matches well with experimental data obtained from thermal gravimetric analysis. Characteristic data for a coating initially about 2-mm thick with a mass-transfer coefficient of 2.4 cm/s are shown in Figure 7. The predicted weight of the coating matches the experimentally measured weight initially, but after cracking occurs in the experiments, the theory deviates from the experiments —and we expect the theory to break down when the coating cracks. More detailed experimental comparison of experiment and theory is discussed by Cairncross et al. (1994).

Effect of varying reaction rates (Damköhler number)

The variations in coating thickness with time based on first-shell substitution on and independent reactions kinetics

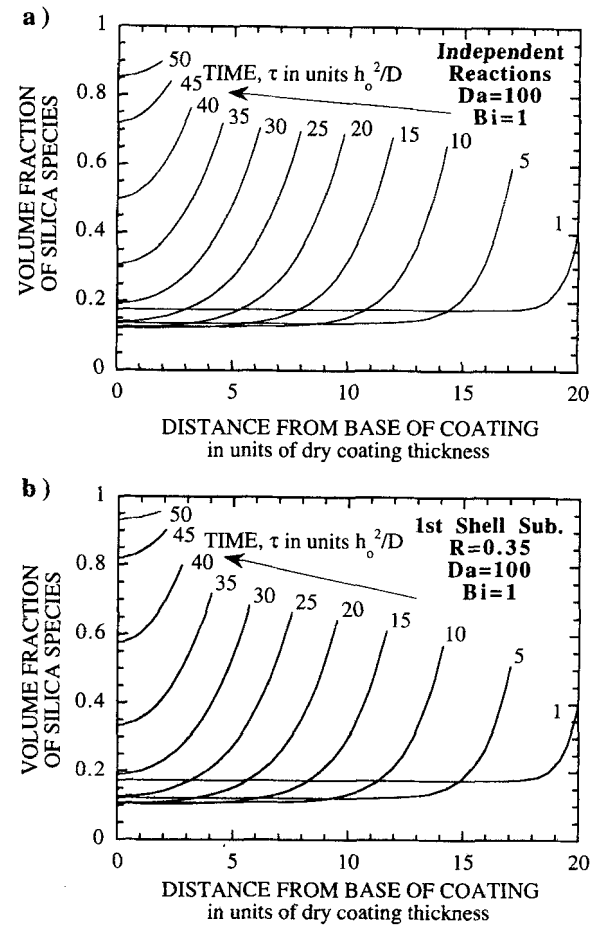

Figure 6. Variation of volume fraction of Si-species through the coating reacting with Damköhler number, $Da = 100$, and Biot number, $Bi = 1$, at a series of time increments.

Results correspond to (a) independent reactions, and (b) first shell substitution ($R = 0.35$).

are shown in Figures 8a and 9a for coatings with varying Damköhler number. The Damköhler number, *Da*, represents the reaction rate in units of the diffusion time, as defined in Table 1. Varying *Da* corresponds to considering reactions in

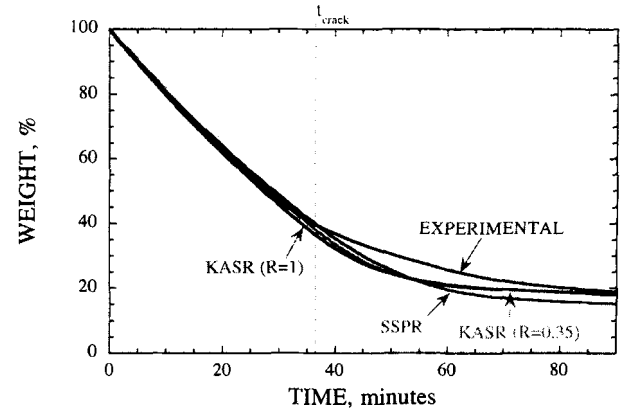

Figure 7. Predicted coating thickness and thickness measured by gravimetric analysis (Cairncross et al., 1994).

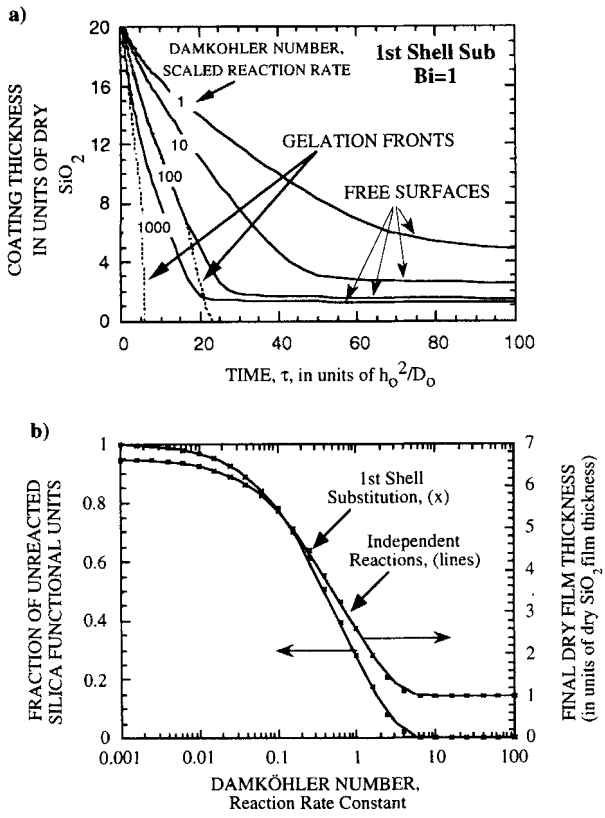

Figure 8. (a) Predictions of coating thickness in a drying coating based on the first-shell substitution reaction scheme and rate constants in Table 1 for a range of Damköhler number, *Da*, at Biot number, *Bi* = 1; (b) fraction of unhydrolyzed functional units after drying is complete as a function of *Da* for *Bi* = 1 and both kinetic schemes.

TMOS at other temperatures, other coating thicknesses, and in other polymerizing systems. Figures 8 and 9 show that coatings with higher reactivity (*Da*) dry faster, which is perhaps surprising. One reason they do is that SiO_2 and TMOS differ in specific volume. A dry coating of TMOS which has not polymerized is about seven times thicker than fully condensed and dried SiO_2 coating as shown in Figure 8b; the thicker coatings have higher diffusional resistance to mass transfer. The final thicknesses among the four cases (Figure 8a) differ because water evaporates completely from the coating before hydrolysis is complete when reactivity is low, but not until after hydrolysis when reactivity is high. If coating porosity is neglected, incomplete hydrolysis reactions produce a partially condensed dry coating that is thicker than a fully condensed dry coating would be.

Water and TMOS accumulate at the free surface because they are less volatile than methanol. Because the reactants are more concentrated at the free surface, the reaction rates there are enhanced (see concentration profiles in Figure 6). Figures 8a and 9a show the gelation front in both the $Da = 100$ and $Da = 1{,}000$ coatings. However, coatings having $Da = 1$ and $Da = 10$ either do not gel at all or gel so slowly that gelation is delayed beyond the time interval shown in Figures 8a and 9a. Thus, several different types of drying and gelation phenomena can be observed at different reaction rate values.

The first derivatives of the thickness profiles in Figure 9a are called the *drying rates* and are shown in Figure 9b; the drying rate represents the rate of shrinkage of the coating, (v^s from Eq. 4). The drying rate curve shows three periods of characteristic behavior: an *early falling rate*, an intermediate *steadying rate*, and a *later falling-rate period*. The steadying-rate period resembles the constant-rate period, which results from externally controlled drying of wetting liquid from a porous medium, or the nearly constant rate period observed in drying of polymeric coatings, which results from wet-bulb-like balance of the rates of heat and mass transfer and evaporative cooling. However, in these results, the steadying-rate period arises from a finite mass-transfer coefficient for mass transport through the gas phase and from an initially high solvent content in the coating. Because the Biot number, or mass-transfer coefficient defined in Table 1, is finite ($Bi = 1$ in Figure 9), the concentration of solvents at the surface of the coating does not go to zero initially (Figure 6). However,

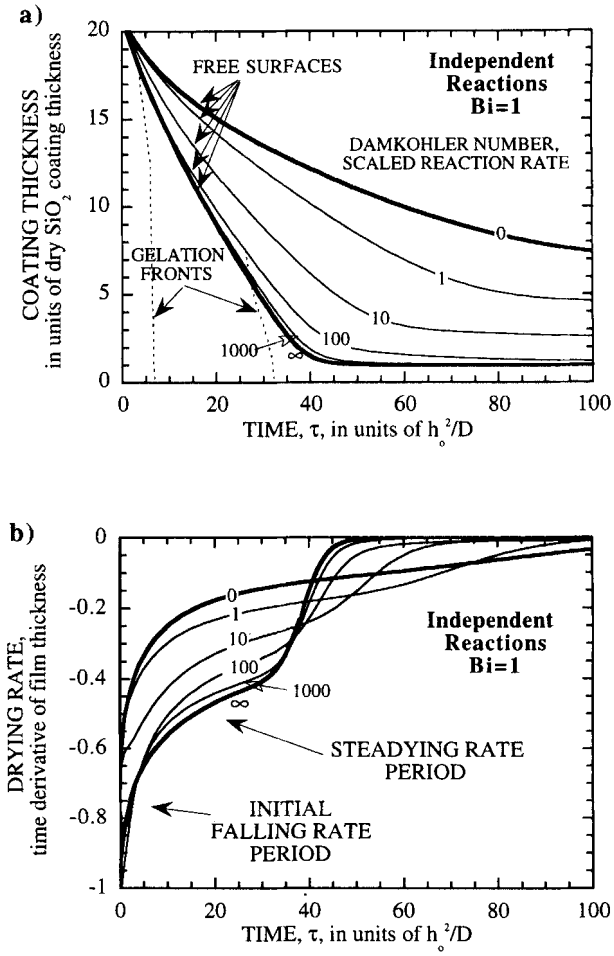

Figure 9. Predictions of a drying coating based on independent reactions and rate constants in Table 1 for a range of Damköhler number, *Da*, at Biot number, *Bi* = 1.

Figures show (a) coating thickness and gelation fronts and (b) drying rate.

the drying rate drops initially because the diffusion of solvents to the surface of the coating does not replenish the solvents lost by evaporation. Then the drying rate falls less steeply in the steadying rate period as the rates of diffusion of solvents to the surface and evaporation of solvents from the surface balance. Eventually, the overall solvent content in the coating drops, and a later falling-rate period develops.

The early falling-rate period is evident only in thick coatings or coatings dried at a high mass-transfer coefficient; this is a period in which the drying rate drops due to high diffusional resistance within the liquid for solvent transfer to the free surface (high *Bi*). In coatings dried slowly enough, the initial drying rate may actually increase due to rapid production of solvents by hydrolysis reactions. The presence and size of these drying periods depends on the parameters, especially the Damköhler and Biot number. The results in Figure 9 all have high enough Biot numbers that an initial falling-rate period exists; however, the duration of the steadying-rate period varies with the Damköhler number. A steadying-rate period does occur in the infinite reaction rate case (completely reacted before drying), showing that the steadying-rate period is independent of the reactions. The results shown here that are based on independent reactions kinetics match well the results based on first-shell substitution kinetics.

Effect of varying drying rate (Biot number)

The type of drying and gelation phenomena predicted depends not only on the reaction rates, or Damköhler number, as shown in Figures 8 and 9, but also on the external mass-transfer rate, or Biot number, as shown in Figure 10, which is based on independent reaction kinetics. In Figure 10a with $Da = 4$, the time to dry the coating and time-to-gelation drop as the external mass-transfer rate rises; between $Bi = 0.3$ to 0.4, the time-to-dry drops sharply and becomes less than the time-to-gelation. In all the results in Figure 10a, the coating gels uniformly, and the gelation time varies between 1,000 and 7,000 (in units of h_0^2/D_0). The time-to-gelation also has a minimum between $Bi = 0.3$ and 0.4. In this range of Biot number, the reactions are significantly enhanced by drying; whereas at higher *Bi*, incomplete hydrolysis causes a delay in the gelation time. Figure 10b shows similar results for faster reactions, $Da = 400$. In this example, the coating always gels before it is dry. At high *Bi*, the liquid near the free surface of the coating gels long before the liquid near the base of the coating, a case of literal skinning, but at low *Bi* the coating gels uniformly. Thus, varying reaction and drying rates creates different types of predicted drying phenomena. These phenomena can be represented on operating diagrams, or drying regime maps, that display regions in parameter space in which the phenomena are predicted.

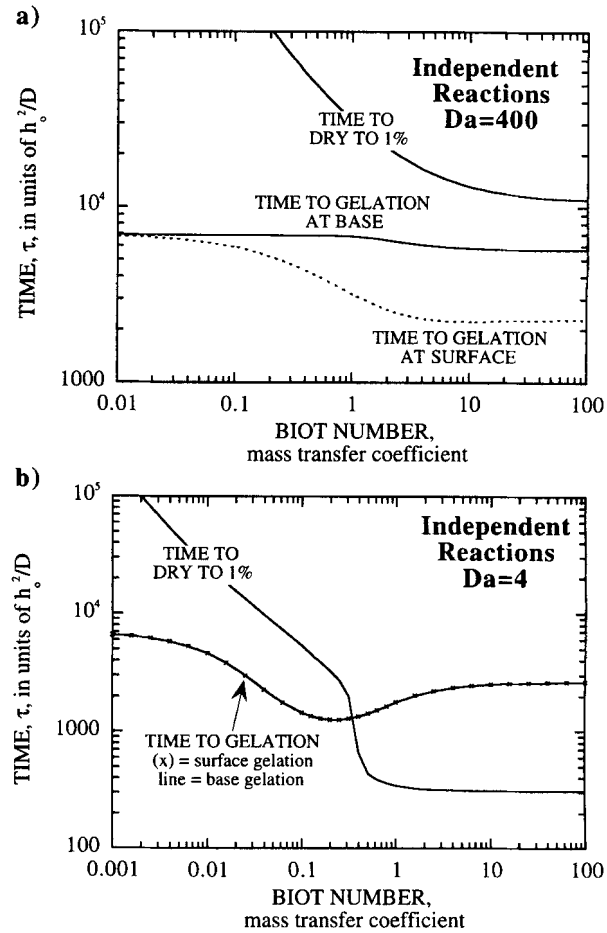

Figure 10. Time-to-gelation vs. time-to-dry to 1% residual solvent over a range of Biot number, *Bi*.

(a) At Damköhler number, $Da = 4$, gelation occurs uniformly. Below $Bi = 4$ gelation occurs before the coating is dry, while above $Bi = 4$ gelation occurs after the coating is dry. (b) At $Da = 400$, literal skinning, a difference in gelation time between the surface and the base of the coating, is evident above $Bi = 0.1$.

Drying Regime Maps

Construction of drying regime maps

As discussed earlier, varying the reaction rate constants and mass-transfer coefficients produces several types of gelation and drying phenomena: gelation before appreciable drying, gelation after nearly all the free solvents are removed, no gelation, and literal skinning (Cairncross et al., 1992). In practice, these phenomena may correspond to different microstructures. For instance, gelation-before-drying is drying of a solid coating, but drying-before-gelation is drying of a liquid coating; most likely *drying-before-gelation* leads to a more dense coating with lower residual stresses than *gelation-before-drying. Literal skinning* is solidification of solution near the surface of the coating while the solution deeper within the coating is still liquid, and literal skinning most likely leads to nonuniform properties. Which phenomena occur depends on the reaction rates, characterized by the Damköhler number; on external mass-transfer rate, characterized by the Biot number; on the kinetic scheme; on the extent of prereaction prior to drying; and on the coating thickness. *Drying regime maps* are diagrams that represent how phenomena depend upon processing conditions.

The location and borders of the regimes are sensitive to their definition. The regime called *no gelation* contains conditions in which gelation does not occur. Regimes of *gelation-before-drying* and *drying-before-gelation* are based on the *time-to-gelation* at the base of the coating relative to the *time-to-dry* the coating. The time-to-dry is the time needed for the coating to reach 1% residual solvent content (integral

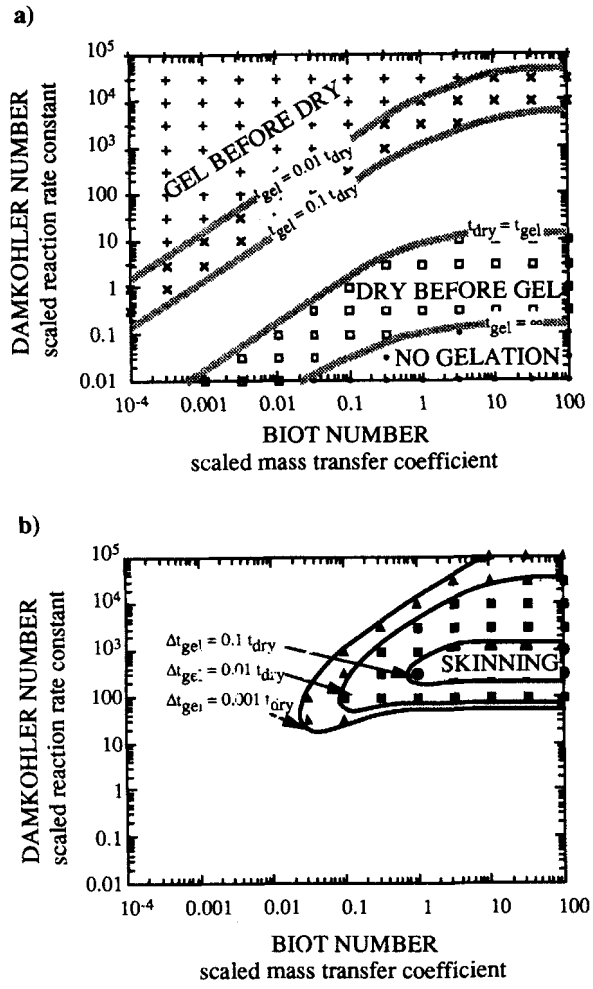

Figure 11. Drying regime maps showing regions of relative drying and gelation times and literal skinning based on independent reactions.

(a) The gray lines indicate approximate contours of constant gelation time as a fraction of the drying time. (b) Black curves are approximate contours of the time lag between gelation at the surface of the coating and gelation at the base of the coating relative to the drying time.

of solvent content through coating). Throughout this article "drying before gelation" denotes results where the time-to-dry the coating is less than the time-to-gel the liquid near the base of the coating; "gelation before drying" denotes results where the time-to-gel the liquid near the base of the coating is less than 10% or 1% of the time-to-dry the coating.

Figure 11a shows how drying and gelation phenomena vary with *Da* and *Bi*. Gelation-before-drying is likely at high *Da* or low *Bi*; whereas drying-before-gelation or no gelation are likely at combined low *Da* and high *Bi*. Points in the figure indicate conditions corresponding to each regime; the lines indicate approximate boundaries between the regions. The boundaries reach limiting asymptotes at high and low *Bi*. At high *Bi*, the drying time is independent of the external drying conditions, and the phenomena depend only upon *Da*. At lower *Bi*, the drying time is inversely proportional to the Biot number because drying is externally controlled, and the phenomena depend upon the ratio *Da*/*Bi*.

The time-to-dry and the time-to-gelation vary by many orders of magnitude throughout parameter space (as shown in Figure 10). Figure 11b displays literal skinning regimes with literal skinning defined by the time lag between gelation at the surface and at the substrate, normalized by the time-to-dry the coating $(t_{gb} - t_{gs})/t_{\mathrm{dry}}$, where t_{gb} and t_{gs} are the times-to-gelation at the base and surface of the coating, and t_{dry} is the time to 1% residual solvent. Literal skinning occurs between the regions of gelation-before-drying and drying-before-gelation at high mass-transfer coefficients—that is, when drying is externally controlled and drying and gelation occur on similar time scales.

Sensitivity of drying regime maps

Figure 12a shows how the drying regimes based on independent reaction kinetics vary with dry coating thickness and external mass-transfer coefficient; this figure shows the same results as Figures 11a and 11b, but the Biot and Damköhler numbers have been converted to mass-transfer coefficient and thickness using their definitions in Table 1. The coating thickness in Figure 12 is the thickness of the dry coating after complete conversion to nonporous SiO_2, that is, it is proportional to the amount of Si in the coating. Figure 12a shows that complete gelation of the coating before it reaches 10% always occurs in dry coatings over 1,000 microns (1 mm) thick. Also, literal skinning is likely in coatings in the range of hundreds of microns thick; whereas thinner coatings tend to gel uniformly either before drying (at low mass-transfer coefficients) or after drying (at high-mass transfer coefficients).

Figures 12a and 12b show drying regime maps based on independent reactions kinetics and first-shell substitution ki-

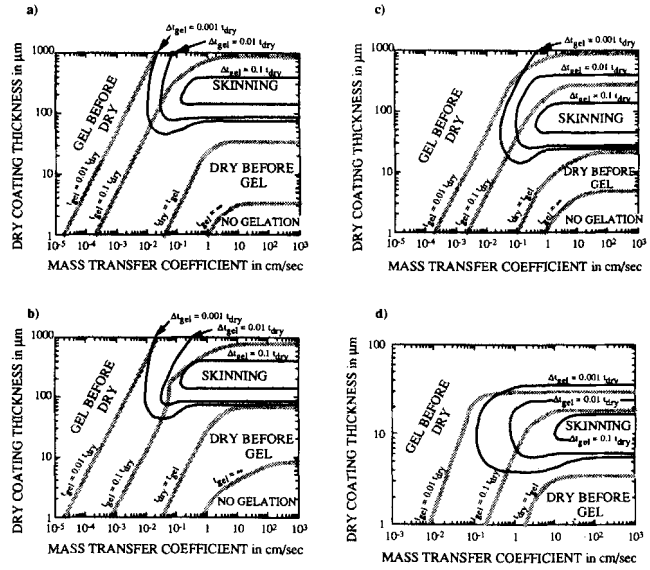

Figure 12. Drying regime map showing regions of literal skinning and relative gelation to drying times as functions of thickness and mass-transfer coefficient (using values in Table 1).

(a) Independent reactions, (b) first-shell substitution kinetics, (c) first-shell substitution kinetics with $R = 1$, and (d) first-shell substitution with $R = 1$, variable diffusion coefficient, and reaction of tetramethoxysilane sol to 10% of gelation time before drying starts.

netics. The literal skinning regions are nearly equivalent. Because drying is faster initially with first-shell substitution (as shown in Figure 5), drying-before-gelation and no gelation occur in thicker coatings, according to first-shell substitution kinetics. Also gelation-before-drying occurs in slightly thinner coatings, according to first-shell substitution. Despite these differences, the overall map based on independent reactions qualitatively agrees with the results based on the first-shell substitution scheme. Because calculations using independent reactions are about ten times faster than those using first-shell substitution, this represents a significant advantage. The resulting Figures 11 and 12 were based on constant diffusion coefficients, sol unreacted initially, and a specific set of kinetics.

Figure 12c shows a drying regime map when there is no first-shell substitution effect. These results, however, are based on the first-shell substitution reaction rate constants of Table 1 with the substitution factor set to $R = 1$. Without substitution, gelation occurs much faster (almost 10 times faster as shown in Figure 4); this causes the regions of gelation-before-drying and literal skinning to shift toward thinner coatings and higher mass-transfer coefficients. The only region that does not change appreciably is the region of no gelation because this region is most dependent upon the hydrolysis rate constant, which is independent of substitution effect (value of R). In Figure 12c, coatings over 30 μm thick either gel before drying or exhibit literal skinning.

Figure 12d shows a drying regime map when there is no first-shell substitution effect (from Figure 12c), but with a concentration-dependent diffusion coefficient, and with *prereaction* of the sol to 10% of the gel time before drying starts. The concentration dependence of the diffusion coefficient is a simple quadratic relationship that loosely approximates the shape of the diffusion coefficient relationships reported in the literature, $D = (D_1 - D_0)x_{Sic}^2 + D_0$, where x_{Sic} is the volume fraction of Si-species condensed at least once. This diffusion coefficient varies by four orders of magnitude between the initial solution and dried SiO_2. This diffusion coefficient dependence is not an attempt to fit real data, but it shows the sensitivity of the results to concentration-dependent diffusion coefficients that are difficult to measure and calculate. In practice, acid-catalyzed TMOS solutions often sit for a specified period between preparation of the sol and coating; this period of time is called *prereaction*. Often, prereaction is a small fraction of the total gel time (less than 10%), but the reactions that take place during this time period affect the gelation phenomena.

In each of the three variations, namely no substitution, concentration-dependent diffusion, and prereaction, coatings gel before drying if they are above 20 μm dry thickness or experience a mass-transfer coefficient below 0.2 cm/s. The concentration-dependent diffusion coefficient lengthens the time-to-dry and prereaction shortens the time-to-gel; so the gelation before drying region shifts to thinner coatings than in Figures 12a–12c. Also in each of the three variants, the lower border of literal skinning is about 5 μm, which is six times thinner than in Figure 12c and twenty times thinner than in Figures 12a, 12b. Thus, Figure 12 shows that the locations of the regions representing different gelation phenomena are sensitive to diffusion coefficients, prereaction, and the type of second-order kinetic scheme, but the general shape of the regions remains the same.

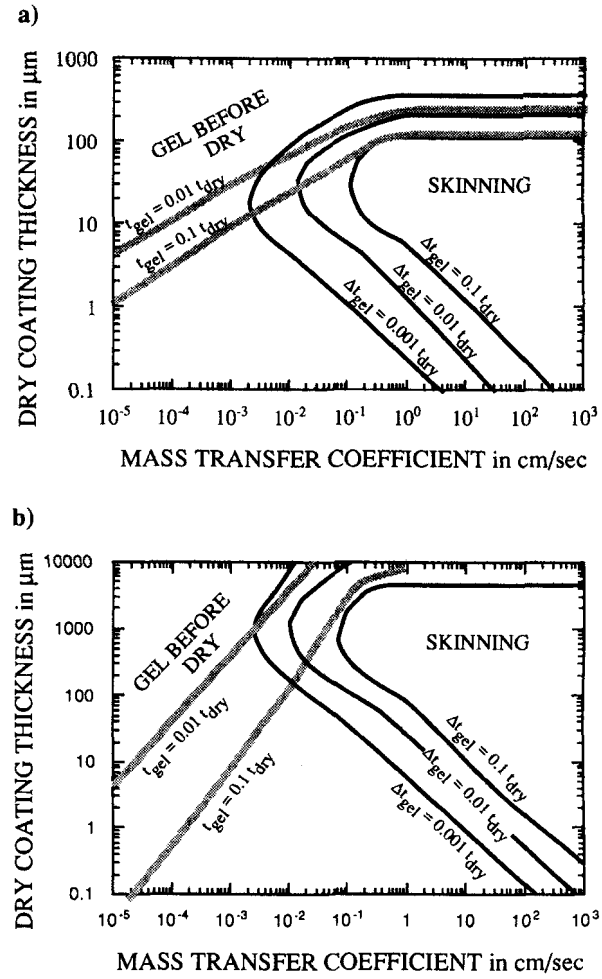

Figure 13. Drying regime map using empirical models for gelation kinetics.

(a) Gelation occurs when the time since mixing is equal to the experimentally measured time-to-gelation (Figure 4, Eq. 9) at the total concentration of silicon species in solution, and (b) gelation reactions occur with first-order kinetics and rate constant defined by Eq. 11 and the data in Figure 4.

The empirical models of gelation discussed earlier (Eqs. 9–11) produce drying regime maps (Figure 13) that contrast with the maps in Figure 12. Because the gelation kinetics in the empirical models depend much more strongly on the solution composition than the second-order schemes predict (Figure 4), drying has a stronger effect on the time-to-gelation. As shown in Figure 13, the empirical models predict literal skinning in coatings much thinner than those shown in Figure 12; coatings well below 1 μm exhibit literal skinning. Also, in the empirical models, gelation kinetics accelerate as the coating nears dryness, so that the dry-before-gelation region is absent in Figure 13 and would not appear until much thinner coatings. Thus, the empirical models predict that coatings with thicknesses that are common in practice would have nonuniform properties.

Discussion

This article discusses phenomena that can occur in drying of coatings that solidify by gelation reactions. The magni-

tudes of reaction rates relative to the mass-transfer rates determine whether gelation occurs before or after most of the solvents have evaporated. The hydrolysis rate constant determines extent of reaction and amount of residual unreacted hydroxide groups that remain in the coating after reaction and drying rates decay to zero. If the hydrolysis rate is high enough, the condensation reactions control the gelation time. The two kinetic schemes examined in this article differ primarily in their prediction of condensation reaction rates. In the Kay and Assink statistical reaction scheme (first-shell substitution), condensation reactions become slower as the polymers condense because the first-shell substitution effect reduces reaction rates ($R < 1$). In the independent reaction scheme, the condensation rate constants are independent of the extent of conversion. Thus, to make the two schemes match on the basis of equal gel time without drying, the condensation rate constants in the independent reaction scheme are lower than in first shell substitution scheme. Consequently, in drying coatings, first shell substitution predicts a faster drying rate initially, because solvent production by initial reactions is faster (Figure 3), and shorter gelation time, because faster drying enhances reactions (Figure 5). Nevertheless, the two kinetic schemes predict that gelation and drying phenomena vary as the parameters in qualitatively the same ways (Figure 10).

However, the predictions of time-to-gelation by these two kinetic schemes do not match well with experimental measurements of time-to-gelation (Figure 4). Although there are several possible reasons for these discrepancies, the kinetic schemes used here are the best available for sol-to-gel solutions. This article demonstrates how to make predictions of coupled drying and reaction, and shows how these results are sensitive to the kinetic scheme.

Drying regime maps represent how drying and gelation phenomena depend upon drying conditions. At low Damköhler number (reaction rate) and high Biot number (drying rate) coatings dry to 1% solvent before gelation of the coating; this corresponds to thin coatings dried at high-mass transfer coefficients that dry as a liquid. At high Damköhler number or low Biot number, coatings gel before solvent removal; this corresponds to either thick coatings or coatings dried slowly that dry as a solid. Between these two extremes, literal skinning, or gelation of the surface of the coating before gelation of the bulk, can occur. If the drying and gelation rates are similar and internal resistance to mass transfer controls drying, then enhanced reactions near the surface cause gelation at the surface of the coating while the rest of the coating is still liquid.

Drying regime maps depend on the kinetic schemes, extent of reaction of the sol prior to drying, and concentration and molecular weight dependence of the diffusion coefficients. The minimum thickness of coatings that exhibit literal skinning shrinks from about 100 μm in a base case to about 5 μm in a coating with prereaction, variable diffusion coefficient, and no substitution effect (Figures 12a and 12d). The empirical models of the gelation kinetics defined in Eqs. 9–11 predict literal skinning to 0.1 μm and below. Thus, improvement in the kinetics and gelation predictions to more accurately describe the sol-to-gel transformation and improvement in the relationship between diffusion coefficient, concentrations, and molecular weight can be expected to shift the literal skinning regions toward thinner coatings.

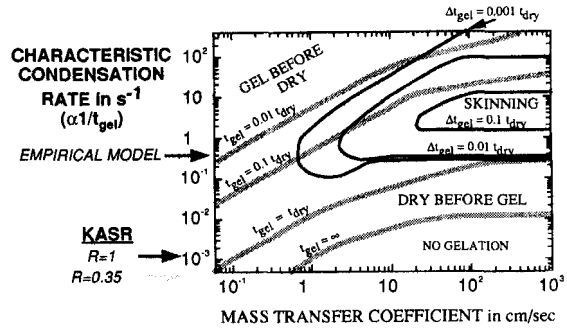

Figure 14. Alternative representation of drying regime map of a 1-μm-thick dry coating.

Results from multiple kinetics schemes are qualitatively represented by characteristic condensation rates.

Figure 14 shows an alternative form of drying regime map that relates the regimes to a characteristic condensation reaction rate and the mass-transfer coefficient in a coating that is 1 μm thick when it becomes dry SiO_2. The data on this plot are the same data as in Figure 11, but the Damköhler number has been converted to a characteristic condensation reaction rate and the Biot number has been converted to the mass-transfer coefficient. Because condensation reactions lead to gelation, the characteristic condensation rate is inversely proportional to the time-to-gelation, as indicated in Eq. 11 for the empirical model. Figure 14 qualitatively represents the data from all three kinetic schemes; arrows to the left of the drying regime map indicate characteristic reaction rates of each scheme. The difficulty in using this figure is that appropriate characteristic condensation rates are required. Because the time-to-gelation is a strong function of the solution composition (Figure 4), the condensation rate varies during the drying process. The characteristic condensation rates corresponding to the arrows in Figure 14 are based on the time-to-gelation at high concentrations of reactants. Thus, Figure 14 qualitatively combines the results from multiple kinetic schemes and pertains to drying and reaction in nonsilicate sol-to-gel coatings as well. Knowing how drying and gelation phenomena depend upon these parameters can help determine the proper drying conditions to achieve a coating of desired properties.

Literature Cited

Abhiraman, A. S., private communication (1994).

Anderson, J. E., and R. Ullman, "Mathematical Analysis of Factors Influencing the Skin Thickness of Asymmetric Reverse Osmosis Membranes," *J. Appl. Phys.*, **44**, 4303 (1973).

Assink, R. A., and B. D. Kay, "Sol-Gel Kinetics: I. Functional Group Kinetics," *J. Non-Crystalline Solids*, **99**, 359 (1988).

Bailey, J. K., C. W. Macosko, and M. L. Mecartney, "Modeling the Gelation of Silicon Alkoxides," *J. Non-Crystalline Solids*, **125**, 208 (1990).

Brenan, K. E., S. L. Campbell, and L. R. Petzold, *Numerical Solution of Initial-Value Problems in Differential-Algebraic Equations*, Elsevier, New York (1989).

Brinker, C. J., and R. A. Assink, "Spinnability of Silica Sols—Structural and Rheological Criteria," *J. Non-Crystalline Solids*, **111**, 48 (1989).

Brinker, C. J., and G. W. Scherer, *Sol-Gel Science*, Academic Press, San Diego (1990).

Brinker, C. J., A. J. Hurd, G. C. Frye, K. J. Ward, and C. S. Ashley, "Sol-Gel Thin Film Formation," *J. Non-Crystalline Solids*, **121**, 294 (1990).

Cairncross, R. A., L. F. Francis, and L. E. Scriven, "Competing Drying and Reaction Mechanisms in the Formation of Sol-to-Gel Films, Fibers, and Spheres," *Drying Technol. J.*, **10**, 893 (1992).

Cairncross, R. A., A. Limbert, L. F. Francis, and L. E. Scriven, "Gravimetric Analysis of Drying Sol-Gel Derived Coatings and Comparison toTheory," *Sol-Gel Processing and Applications*, Plenum Press, New York, p. 111 (1994).

Cairncross, R. A., "Solidification Phenomena During Drying of Sol-to-Gel Coatings," PhD Thesis, Univ. of Minnesota, Minneapolis, (1994). (Available from University Microfilm International, Ann Arbor, MI.).

Calbo, L. J., *Handbook of Coatings Additives*, Marcel Dekker, New York (1987).

Cohen, E. D., "Coatings Going Below the Surface," *Chem. Eng. Prog.*, (Sept., 1990).

Crank, J., and G. S. Park, "Diffusion in High Polymers: Some Anomalies and Their Significance," *Trans. Farad. Soc.*, **47**, 1072 (1951).

Cussler, E. J., *Diffusion and Mass Transfer in Fluid Systems*, Cambridge Univ. Press, New York (1984).

Finlayson, B. A., *Numerical Methods for Problems with Moving Fronts*, Ravenna Park, Seattle, WA (1992).

Flory, P. J., *Principles of Polymer Chemistry*, Cornell Univ. Press, Ithaca, NY (1953).

Frisch, H. L., "Sorption and Transport in Glassy Polymers—A Review," *Poly. Eng. Sci.*, **20**, 2 (1980).

Hahn, F. J., "Cratering and Related Phenomena," *J. Paint Technol.*, **43**, 58 (1971).

Kay, B. D., and R. A. Assink, "Sol-Gel Kinetics: II. Chemical Speciation Modeling," *J. Non-Crystalline Solids*, **104**, 112 (1988).

Limbert, A., private communication (1993).

Long, F. A., and D. Richman, "Concentration Gradients for Diffusion of Vapors in Glassy Polymers and their Relation to Time Dependent Diffusion Phenomena," *J. Amer. Chem. Soc.*, **82**, 513 (1960).

Macosko, C. W., and D. R. Miller, "A New Derivation of Average Molecular Weights of Nonlinear Polymers," *Macromol.*, **9**, 199 (1976).

Ng, L. V., P. Thompson, J. Sanchez, C. W. Macosko, and A. V. McCormick, "Formation of Cagelike Intermediates from Nonrandom Cyclization During Acid-Catalyzed Sol-Gel Polymerization of Tetraethyl Orthosilicate," *Macromol.*, **28**, 6471 (1995).

Petzold, L. R., "Differential/Algebraic Equations are not ODE's," *SIAM J. Sci. Stat. Comput.*, **3**, 367 (1982).

Pierce, P. E., and C. K. Schoff, *Coating Film Defects*, Federation of Societies for Coatings Technology, Philadelphia (1988).

Powers, G. W., and J. R. Collier, "Experimental Modelling of Solvent-Casting Thin Polymer Films," *Poly. Eng. Sci.*, **30**, 118 (1990).

Sanchez, J., and A. V. McCormick, "Kinetic and Thermodynamic Study of the Hydrolysis of Silicon Alkoxides in Acidic Solutions," *J. Phys. Chem.*, **96**, 8973 (1992).

Sanchez, J., and A. V. McCormick, "Intramolecular vs. Intermolecular Condensation Rates in the Acidic Polymerization of Octaethoxytrisiloxane Solids," *J. Non-Crystalline Solids*, **167**, 289 (1994).

Sanchez, J., S. E. Rankin, and A. V. McCormick, "^{29}Si NMR Kinetic Study of Tetraethoxysilane and Ethyl-substituted Ethoxysilane Polymerization in Acidic Conditions," *Ind. Eng. Chem. Res.*, **35**, in press (Jan., 1996).

Strang, G., and G. J. Fix, *An Analysis of the Finite Element Method*, Prentice-Hall, Englewood Cliffs, NJ (1973).

Tsay, C. S., and A. J. McHugh, "Mass Transfer Modeling of Asymmetric Membrane Formation by Phase Inversion," *J. Poly. Sci.: Part B Poly. Phys.*, **28**, 1327 (1990).

Vrentas, J. S., and J. L. Duda, "Diffusion in Polymer–Solvent Systems," *J. Poly. Sci.: Poly. Phys. Ed.*, **15**, 403 (1977).

Vrentas, J. S., J. L. Duda, and H.-C. Ling, "Enhancement of Impurity Removal from Polymer Films," *J. Appl. Poly. Sci.*, **30**, 4499 (1985).

Manuscript received Aug. 23, 1994, and revision received Feb. 6, 1995.